e-Prime - Advances in Electrical Engineering, Electronics and Energy 3 (2023) 100093

Contents lists available at ScienceDirect

e-Prime - Advances in Electrical Engineering, Electronics and Energy

journal homepage: www.elsevier.com/locate/prime

Optimizing the Performance of Single-Phase Photovoltaic Inverter using Wavelet-Fuzzy Controller

Mohammed Ali Khan [a,*], Ahteshamul Haque [b], Varaha Satya Bharath Kurukuru [c], Frede Blaabjerg [d]

[a] Department of Electrical Power Engineering, Brno University of Technology, Brno, Czech Republic
[b] Advance Power Electronics Research Lab, Department of Electrical Engineering, Jamia Millia Islamia, New Delhi, India
[c] Research Division Power Electronics, Silicon Austria Labs GmbH, Villach, Austria
[d] AAU Energy, Aalborg University, Aalborg, Denmark

ARTICLE INFO

Keywords:
Solar inverter
H5 transformerless topology
Wavelet transform
Fuzzy logic control
Total harmonic distortion
Standalone inverter

ABSTRACT

During grid-connected operation, photovoltaic (PV) systems are usually operated to inject pre-set power to the grid. However, when the main grid is cut off from the PV system, standalone operation must be achieved while operating in voltage control mode. This brings new challenges for the control of PV inverters, i.e., voltage regulation and harmonic elimination. In this research, a wavelet-based fuzzy control for standalone operation of single-phase inverters is designed. The proposed controller regulates the output voltage by adjusting the fuzzy controller weights, which are operating in closed loop with the pulse width modulation generator. A hardware prototype of 1kWp standalone PV system is developed, and the proposed control method is evaluated on it. The proposed control achieves < 6 % of output voltage regulation under steady state and step load conditions while reducing total harmonic distortion (THD) for steady state condition. The THD of the proposed system operating with linear loads is observed to be 2.18%, and for nonlinear loads, it is around 2.71% under simulation conditions.

1. introduction

The implementation of photovoltaic (PV) systems in the power grid is accepted on a wide scale due to the development in technology aiding for clean energy, and environmental safety. While operating in a grid-connected mode, the distributed generation (DG) injects pre-set power into the grid through a current control mode in synchronization with the grid [1]. During grid faults, the power electronics integrating the PV with the grid must be capable of supporting the grid for a certain time and protect its DG by disconnecting from the grid. When the DG system is disconnected from the grid, intentional islanding or standalone operation can occur, where the DG system needs to regulate the local loads in a voltage control mode [2,3]. This will create an imbalance in the system voltage and generates harmonics during operation resulting in power quality problems and system instability. In addition to the voltage regulation problem faced during the standalone mode of operation, the ability of the system to automatically readjust to load variations, such as load shedding, brings a challenge because of the assumption that there is no previous knowledge of the loading levels.

To solve the issue regarding the islanded or standalone operation, an efficient control algorithm is required for achieving voltage regulation. Initially, cascade-based control structures [4], were adapted in two layers, where one layer controls the active and reactive power, and the other layer controls the frequency and load voltage [5]. Further mode transition control [6], resonant control [7], logic control [8], droop [9], and vector control [10] are usually employed. There are certain challenges regulating the transients in load voltage especially while dealing with the nonlinear loading. This resulted in the need for the development of advanced voltage control schemes, which can ensure stable operation and achieve low total harmonic distortion (THD). A load current observer-based model predictive controller is developed in [11], but was limited in performance due to non-substantial improvement reported in high THD. Further, repetitive control schemes [12] are developed with an aim to reduce the value of THD under uncertain load condition. The system is robust, but a certain delay can be observed in the system when a transient response is considered. These drawbacks were overcome by adapting feedback linearization controllers [13], flatness-based controller techniques [14] and sliding mode controllers

* Corresponding author

https://doi.org/10.1016/j.prime.2022.100093

Available online 30 November 2022

[15] where the current prediction takes place at the outer loop and current control occurs at the inner loop. In [16], a model predictive controller is designed for achieving the standalone operation of a single-phase split source inverter. The experimental THD of the inverter with the developed control approach is reasonable high despite low value during the simulation phase. Besides, the research didn't consider the operation of the developed controller with a nonlinear load. Further, a direct sliding mode controller is designed in [17] for overcoming the dynamic instabilities in the standalone operation of a PV system. The contribution is focussed at minimizing the size of the DC link capacitor and doesn't emphasize on the overall efficiency of the converter with the developed control approach. In [18], the standalone operation of a PV system is achieved with an indirect closed loop control of a quasi-z-source inverter. Here, the control methodology used a single loop Pi controller at the DC side which is identified to have drawbacks due to sensitivity of the control gains to transients in the system outputs. Furthermore, a brief overview of various control approaches designed for standalone operation of a single-phase standalone inverter is summarised in [19].

From the above observations, the overall inability of controllers in regulating the transients in load voltage and achieving low THD is still a major drawback, especially while operating with nonlinear loads during standalone mode. Recently intelligent control techniques have become the most reliable and fast recovering mode of control islanded operation of DG systems [20]. Hence, the proposal of an optimized intelligent controller using fuzzy logic control (FLC) for voltage loop control of inverters is developed. The drawback of identifying the transient variations in the load voltage especially during islanded or standalone operation and load varying processes resulted in the need for optimizing the FLC. Besides, FLCs have difficulties in determining the appropriate control laws and tuning the parameters of the membership function according to the changes in the system. Hence, to overcome this, intensive research is done on the optimization, design and implementation of FLC with neural network controllers and other heuristic search algorithms [21–25]. But the serious drawback with most optimized fuzzy methods is, they often furnish rules without a transparent interpretation and involve approximate model parameters in the design. This resulted in large settling time which eventually turns out to be a drawback while dealing with transients during load switching in standalone operation of DG systems. Moreover, literature has reported work on the use of time frequency localization of wavelet transform (WT) for inverter control to achieve speed control of electrical drives [26,28]. In [26], a single phase voltage source inverter is operated with a wavelet based modulation technique. Here, the switching pulses are generated using multi-resolution analysis based nondyadic wavelet functions. The developed approach adjusted the locations of zero-crossing in the first derivative of reference modulating signal to vary the scales of shifted and dilated scaling functions. Further, in [27, 28] the authors established a maximum value for scaling functions to generate the wavelet modulated inverter switching signals for singe phase and three phase inverters. In [29], the multi resolution wavelet modulation scheme is developed to reduce the electro-magnetic interference by improving the output harmonic frequency spectrum. Here, the behavior of inverter modulation scheme is realized by the multi resolution analysis developed by combined Haar wavelet basis functions. This models the wavelet as a non-uniform recurrent sampling and reconstruction process.

From the above studies, it is identified that, WT can decompose wide band signals into time and frequency localized sub bands. Further, combining WT with intelligent techniques such as fuzzy logic yields particularly reliable results in the high-performance applications of the inverters. The main objective of this work is to develop and implement a wavelet based fuzzy controller for the control of an inverter. In this hybrid controller, the discrete wavelet transforms (DWT) are used to decompose the error between the measured and the reference output voltages into different frequency sub bands. These transformed sub band coefficients are scaled by their respective gains and then combined to generate the control signal. This novelty of the proposed wavelet based fuzzy scheme for inverter control is defined by:

- The firmness of the WT provides an advantage by processing and analysing the signal through math series representation.
- The controller when operated with H5 transformerless inverter depicted fast execution, enhanced performance, and stability for the system.
- The developed controller regulates the load voltage within the limits while operating with both linear and non-linear loads.
- The regulated voltage output corresponds to reduced harmonics, hence improving the efficiency of the inverter.

Besides, the tolerance of the controller towards transients in load voltage and current during the load variation is achieved with the superior noise rejection capability of the DWT based control approach. This is one of the major advantages of the proposed controller over the conventional methods.

The paper is organised as follows: Section 2 provides brief details about standalone PV systems, their components, and operation. Section 3 introduces the wavelet fuzzy controller and field programmable gate arrays (FPGA) implementation of the developed controller. Section 4 presents the validation of the developed controller with the help of simulation and laboratory prototype experiment and the corresponding results are concluded in Section 5.

2. System DESCRIPTION

2.1. Stand-alone photovoltaic systems

Generally, PV systems are classified according to the mode of operation: standalone or grid connected. In standalone applications, the PV system supports the loads assigned to it, either with the help of a battery and/or other energy storage devices. In grid-connected operation, the PV system is integrated with the grid to support the loads associated both with the grid as well as with the PV system. Whenever, a grid fault occurs or during grid maintenance, the PV inverter should be able to disconnect the PV system from the grid and support its local load by operating in standalone mode, as allowed by the grid utility manager to minimize outages.

Therefore, the standalone mode operation of a PV system is of almost importance with the control of the inverter to be performed efficiently. The major components of a standalone PV system are, a PV array with maximum power point tracking (MPPT) based DC-DC converter, and inverter with output filter. The DC-DC converter, along with a dedicated MPPT algorithm plays a major role in extracting maximum power from the PV array during varying irradiation conditions. Detailed information on MPPT algorithms have been proposed and implemented in [30,31]. This research adapts perturb and observe (P&O) algorithm for performing the MPPT operation. This maintains the dc link voltage at the input terminals of the inverter as per the DC-DC converter rating; in this research, a Boost converter is used.

2.2. Transformerless inverter topology

The transformerless inverter topology is realized by adapting an H5 inverter topology [32]. In the H5 inverter topology, a switch S5 is connected as DC bypass in the presence of four switches S1 to S4. The operation of S1 and S4 occurs at the system line frequency, whereas S2, S3, and S5 operate at a higher frequency. The S5 switch disconnects the solar panel during freewheeling of the half-bridge inverter. The S1 switch closes the freewheeling path by an inverse diode of S1 and S3 during the negative half of the period [33]. The mode of operations is taken as two freewheeling modes and two operational modes. During the operational modes, the switches have a direct current inflow from

the panel whereas, in freewheeling mode the switch at the DC link restricts the flow of current.

Mode 1 and 3- S1 and S4 Switch operates at a switching frequency. The S1 switch is turned ON continuously for the first half whereas S3 operates during the negative cycle. Between S4 and S5 high-frequency switching was carried out for obtaining positive voltage vector. In case of the negative vector for mode 3, high frequency switching of S2 and S5 is performed. For the operation of mode 1, the S1 and S4 switch is turned on, and flow of current is taking place from S5 to S1 and returning via S4. Whereas in mode S3 switch is turned on, and a current path is created from S5 to S3 and returning from S2.

Mode 2 and 4- During freewheeling mode, S4 and S5 are off, and freewheeling take place in between S1 and S3 switches. Further, high filtering is required as switching ripple in the current is equal to switching frequency. The efficiency of the H5 topology is higher than the regular inverter even though one more transistor is required. The switch S1 operates at a higher frequency for both positive and negative cycles as a reference is a sinusoidal wave. Fig. 1 shows the H5 transformerless inverter topology along with the filter implementation. A mathematical model of the H5 transformerless inverter is presented in literature [34] and the switching program is given through Fig 2.

To obtain the fundamental frequency output from the inverter, a low pass filter needs to be adapted [35]. A third order LCL filter is utilized in both stand alone as well as grid-connected systems because of its high attenuation value beyond resonating frequency. For designing an LCL filter, various parameters such as current ripple through inductor and filter resonance need to be considered. The design aspects required for an LCL filter are adopted from [36,37]. As per [37], the inductor (L_1) in accordance with the maximum permissible ripple current in the converter is given by:

$$L_1 = \frac{v_{dc}}{4.f_{sw}.\Delta I_{L_{max}}} \tag{1}$$

where, v_{dc} is the voltage across the DC link capacitance, f_{sw} is the switching frequency, and $\Delta I_{L_{max}}$ is selected as 10 % of the rated converter current. Further, the filter capacitance C_f is obtained as follows (2):

$$C_f \leq 0.05.\frac{P_n}{\omega_f.V_n^2} \tag{2}$$

where, P_n is converter rated power, ω_f is the angular frequency, and V_n is the nominal RMS voltage at the load. The filter capacitance should be $\leq$ 5 % of the base capacitance value. The basis for selection of load side inductor is given by:

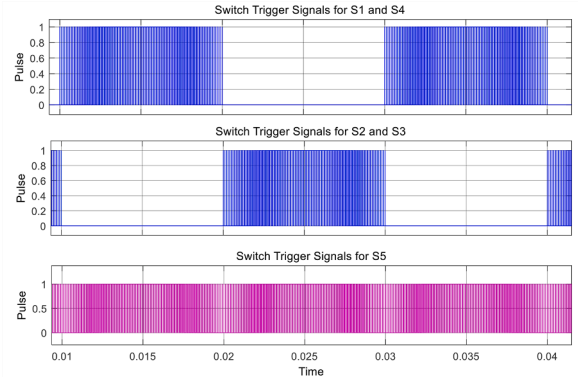

Fig. 2. Switching program for H5 transformer less inverter.

$$L_2 = \frac{sqrt\left(\frac{1}{k_a^2}\right) + 1}{C_f.2.\pi.f_{sw}} \tag{3}$$

where, k_a is the required attenuation.

The maximum value of total inductance $(L_1 + L_2)$ should be below 10 % of base value to avoid large voltage-drop across the inductor (4).

$$L_1 + L_2 < 10\ \% \left(\frac{V_n^2}{2.\pi.f_g.V_{rated}^2}\right) \tag{4}$$

The specifications of stand-alone PV system used in this research, are mentioned in Table 1. The values of the LCL filter are calculated depending on installed PV array capacity, DC link voltage and switching

Table 1
Design parameters for standalone PV system.

Parameter	Value
PV Array	1kWp
Boost Converter	5 kHz,500 V
MPPT	P&O
DC-link proportional integral (PI) controller	$K_{\_p}$ = 0.01, K_I=0.5
DC-link voltage	400 V
Switching frequency	5kHz
Converter side Inductance L_1	3.809 mH
Load side Inductance L_2	2.021 mH
Filter Capacitance C_f	3.0101 uF
Peak voltage	339.36 V
RMS load voltage	V_n=240 V

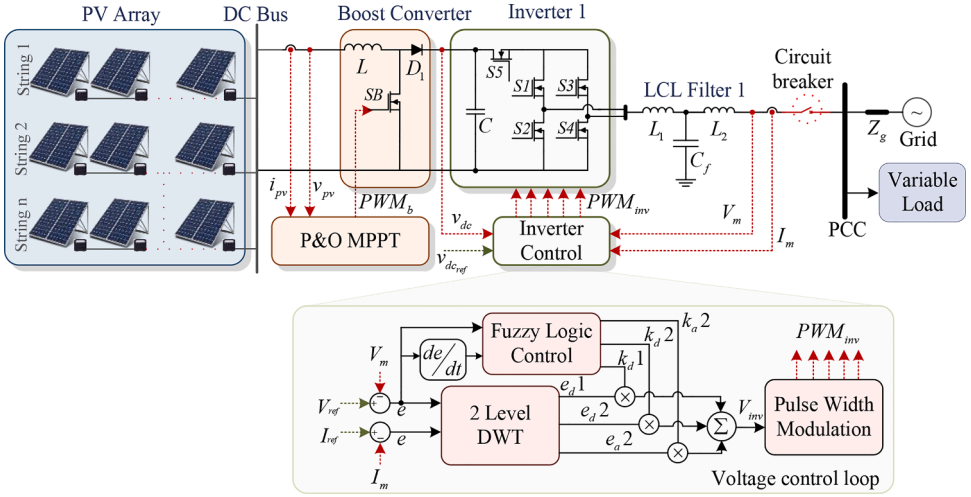

Fig. 1. Standalone operation of H5 transformerless inverter with proposed control topology.

frequency as mentioned in (1) to (4). The controller implementation is tested with linear and nonlinear resistive loads.

2.3. DC link control

As the PV array is defined as a DC current source, and there is a capacitor connected in parallel with it representing the DC link, there are two scenarios that are to be considered with this arrangement. The first scenario, no current passes through the inverter to the load with, the DC current source feeding the DC link capacitor. The relation between capacitor voltage and current is given by:

$$i_{dc} = C\frac{dv_{dc}}{dt} \tag{5}$$

where, the capacitor voltage is denoted by v_{dc}. From (5), it can be identified that, for a constant DC current, the voltage ramps up to infinity or until the capacitor is destroyed. In the second scenario, due to high power transfer from DC side to inverter terminals, the DC link voltage will sink below the general voltage requirements given in (6):

$$v_{dc} + v_{dc}(t) > v_m(t) \tag{6}$$

During this scenario, the clipping of voltage output occurs, and the current output injects harmonics into the load. Hence the need for controlling the current magnitude arises to regulate the dc bus voltage to a nominal value. The control method calculates the voltage error to regulate the current magnitude. A basic PI controller is used for this operation of DC link voltage control and the controller development is illustrated in Fig. 3.

The low pass filter attenuates the double frequency ripple in the measured DC voltage to speed up the controller. The saturation ensures the normal operation of capacitor for conditions where the error is positive. Further, the zero-order hold ensures that no capacitor voltage ripple is passed to the current magnitude command. The complete operation regulates the dc link while the power flows from PV to the load.

3. Control ALGORITHM

3.1. Motivation for using wavelet fuzzy

Considering high power applications, especially in the case with nonlinear loads, it is difficult to minimize the voltage distortion because of the relative high output impedance. In addition, the conventional soft switching methods are also prone to imprecise control because of the soft switching interventions, which causes dwell time in the techniques. These drawbacks motivated the study and design of wavelet-based fuzzy control method. The advantage of the wavelet fuzzy controller is that it processes and analyzes the signal through a math series representation. The process results in fast execution, enhanced performance, and stability of the system. In addition, the tolerance of the controller towards system fluctuations and the superior noise rejection capability are major advantages of the proposed controller over conventional methods.

3.2. Wavelet transform

The WT is a spectral analysis method which decomposes a signal into a set of oscillatory functions called wavelets. These wavelets are localized in time, and thus, provides a time-frequency representation. In this section, the focus will be on the DWT, which is commonly used for signal analysis. The DWT provides a non-redundant representation of a signal with the help of a set of discrete orthonormal wavelets. These set of wavelets are derived from a function called the mother wavelet, commonly denoted as ψ. For any given signal $x(t)$, as such, the DWT representation can be given as:

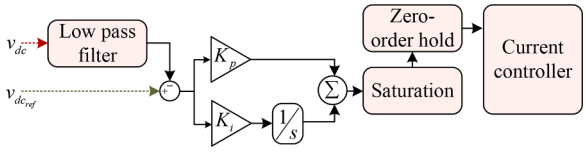

Fig. 3. DC link voltage regulation with PI controller.

$$WT_{m,n}x(t) = \int_{-\infty}^{\infty} x(t).\psi^*_{m,n}(t)dt \tag{7}$$

where, $\psi^*_{m,n}(t)$ is wavelet function with m and n corresponding to dilatation and translation parameters.

To implement the DWT, a cascade stage of low pass and high pass filters is realized. This structure is trailed by down sampling, resulting in a frequency dilation. In general, the low pass filter provides an approximate coefficient for the signal, whereas the high pass filter provides a detailed coefficient. For a first level decomposition, the approximate coefficient a^1 and detailed coefficient d^1, are mathematically derived from (8) and (9) [38]:

$$a^1[n] = \sum_{k=0}^{N-1} g[k].x[n-k] \tag{8}$$

$$d^1[n] = \sum_{k=0}^{N-1} h[k].x[n-k] \tag{9}$$

where $h[k]$ and $g[k]$ denotes wavelet coefficients.

From the first level of decomposition, the approximate coefficients are given as inputs to the down-sampled filters. At this stage, the second level decomposition is performed. The approximate coefficient a^2 and detailed coefficient d^2 are mathematically obtained as depicted in (10) and (11)

$$a^2[n] = \sum_{k=0}^{\frac{N}{2}-1} g[k].a^1[2n-k] \tag{10}$$

$$d^2[n] = \sum_{k=0}^{\frac{N}{2}-1} h[k].a^1[2n-k] \tag{11}$$

This process is continued till the desired level of sampling is achieved.

3.3. optimal selection of wavelets

Selection of mother wavelet along with scaling and wavelet functions plays a major role in developing the wavelet fuzzy controller. Desirable properties of wavelet functions are its orthogonality, compactness, linear phase, and low approximation error, etc., [39]. Less computation effort is required for wavelet functions because of its compactness. The detection of the frequency component of the signal helps in designing the voltage compensator for the inverter. To achieve this, the minimum description length (MDL) data criterion [40] is identified to be the most suitable for selection of an optimum wavelet function. The advantage of MDL over other qualitative wavelet selections approaches is its ability to prevent over/under fitting the data and facilitate an optimal model order selection for estimating the global trend. It also helps in designing a superior wavelet filter for signal decomposition which provides the shortest description of the data model. Further the MDL model can be defined as (12) [41]:

$$MDL(k,n) = min\left\{\frac{3}{2}.k.logN + \frac{N}{2}.log\left|\left|\bar{a}_n - a_n^k\right|\right|^2\right\} \tag{12}$$

$$0 \le k < N;\ 1 \le n \le F;\ \bar{a}_n = 0$$

Where, k and n denote the indices. The integers N and F are the signal length and the wavelet filters utilized, respectively. k denotes the number of coefficients, as a result that MDL criterion gives the minimum value which is considered as the optimum one.

Apart from the choice of wavelet coefficients, the appropriate level of decomposition is necessary. Depending upon the level of decomposition, the optimization parameters for wavelet-based controller is chosen. In general, the maximum number of levels possible for decomposing a signal (L_{max}) is determined based on the sampling frequency N, and decomposition filter length N_W as (13)

$$L_{max} = \text{fix}(\log[(N / N_W) - 1]) \tag{13}$$

where N_w gives the length of the decomposition filter associated with the chosen mother wavelet and fix is to round the value in the brackets to its nearest integer. Besides, it was observed that Shannon entropy-based criterion can also be used for identifying the levels of decomposition for a signal. Here, the entropy of a signal $x(n) = \{x_1, x_2, x_3, \ldots, x_n\}$ of length N can be represented as (14) [41]:

$$H(x) = -\sum_{n=0}^{N-1} |x(n)|^2 .log|x(n)|^2 \tag{14}$$

As per the Shannon entropy-based criterion, if signal entropy at a new level p is higher than the previous level $(p-1)$, then it is depicted as (15)

$$H(x)_p \geq H(x)_{p-1} \tag{15}$$

Hence, the decomposition of the signal may stop at a level $(p-1)$, which is an optimum decomposition level.

3.4. Wavelet fuzzy controller

Once the signal decomposition is achieved, the obtained approximated and detailed coefficients are used for calculating the parameters required for a wavelet-based controller. These aspects are mathematically depicted as in (16) given by [42]:

$$u_w = K_{d^1} e_{d^1} + K_{d^2} e_{d^2} + \ldots..K_{d^N} e_{d^N} + K_{a^N} e_{a^N} \tag{16}$$

Where u_w is the controlled output of the wavelet fuzzy, the detailed components of the error signal are denoted by $e_{d^1}, e_{d^2}, \ldots, e_{d^N}$ and the approximate component is given by e_{a^N}. The gain values $k_{d^1}, k_{d^2}, \ldots, k_{d^N}$ are used for tuning of medium and high frequency components of the error signal and the low frequency components are tuned using the gain value of k_{a^N} [43].

While dealing with inverters, the disturbances are generally low frequency signals, and the sensor measurement noises are high frequency signals. Hence, the gain value for corresponding low frequency component of the error signal can be utilized for improvement of the disturbance rejected by the signal. The value of gain for related to high frequency component can be minimized by elimination of noise impact of the system [44].

Fig. 1 depicts a wavelet-based fuzzy scheme for inverter voltage regulation. The difference between measured voltage (Vm) and reference voltage (V_{ref}) value acts as an error signal, which is an input for both wavelets transform and fuzzy logic-based control block. The error signal is sampled at a frequency of $1e^4$ and the corresponding frequency band ranges from 512 Hz to. Usually, the negative frequency is neglected for the real signals. Further, the signal is decomposed by the 2 level DWT into various detailed and approximate control. The first level of decomposition corresponds to an approximate coefficient of frequency band 0–256 Hz, and the detailed coefficient has a frequency band of 512–256 Hz. Similarly, the second level has approximated and detailed coefficients in the frequency band of 0–128 Hz and 256–128 Hz , respectively.

Parallelly, depending on the voltage error and its derivative fuzzy controller generate a gain value k_d^1,k_d^2 and k_a^2 and respective frequency component of e_d^1,e_d^2 and e_a^2, The frequency component is multiplied along with the scaling gains, and they are concluded together to generate a control signal for inverter. The fuzzy rules, fuzzification and defuzzification interface together form FLC control block. Error in voltage and change in error are two inputs which are fed to FLC block. The process of fuzzification consists of five Mamdani membership functions for both the inputs and outputs which are normalized between −1 and 1 as shown in Fig. 4 and the operating rules of fuzzy are given in Table 2. The linguistic members in Fig. 4 and Table 2 correspond to very large (VL), large (L), medium (M), small (S) and very small (VS). The FLC output comprises of scaling gain which is combined along with corresponding WT for generating pulses which are utilized for inverter output control.

3.5. Stability analysis

The scaling gains of the fuzzy controller have been determined and updated by the action of the WT. The stability of the proposed controller depends on the performance of the optimized FLC algorithm. Hence, a passivity in approach is adopted to determine the absolute stability of the fuzzy controller. This approach is based on some general characteristics of the input-output mapping of the controller and the input-output dynamics of the controlled system [45]. The mapping between the input and output of the fuzzy logic can be in general described as (17):

$$u_k = \frac{\sum_{i,j}\left[\left(\mu_{E_i}(e_1) \cap \mu_{E_j}(e_2)\right).u_{n(i,j)}\right]}{\sum_{i,j}\left(\mu_{E_i}(e_1) \cap \mu_{E_j}(e_2)\right)} \tag{17}$$

where, e_1 corresponds to error $e(k)$ at time k, e_2 corresponds to change in error $de(k)$ at time k, u_k represents the output of the FLC, E_i, E_j and $u_{n(i,j)}$ are the linguistic variables of e_1, e_2 and u_k, respectively, and $\cap$ represents a fuzzy set intersection operator.

Hence, the distinguishing characteristics of the FLC in this work are:

1) In the fuzzy rule matrix, the control rules are anti-symmetric about its off diagonal (odd symmetry).
2) The fuzzy table numerical values increase/decrease gradually from top to bottom in a column and left to right in a row (monotony).
3) The central element of the rule table which corresponds to a control decision is usually zero and the elements surrounding the central area have small values.

These properties of the fuzzy controller reflect the consistency of operator control action and reflect the general properties of the system.

Moreover, the output u of the scalar controller is estimated by center average defuzzification using min operator as follows:

$$u = \Phi(e_1, e_2) = \frac{\sum_{i,j} U_{f(i,j)} \min\left[\mu_{E_i}(e_1), \mu_{E_j}(e_2)\right]}{\sum_{i,j} \min\left[\mu_{E_i}(e_1), \mu_{E_j}(e_2)\right]} \tag{18}$$

Besides, the properties of input-output nonlinear mapping described based on the continuous-time Lipschitz function $\Phi(.,.)$ are given as:

Property a: $|\Phi(e_1, e_2)| \leq u_M$ and $M = \max_{i,j} U_{f(i,j)}$

Property b: $\Phi(0,0) = 0$ defines the steady-state condition.

Property c: $\Phi(e_1, e_2) = -\Phi(-e_1, -e_2)$ defines the odd symmetry

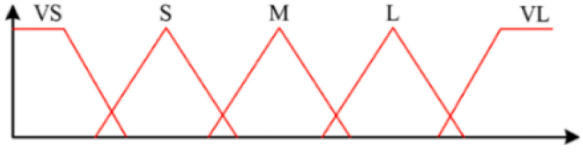

Fig. 4. Membership functions for inputs and outputs of the fuzzy controller.

Table 2
Rules for operation of fuzzy controller.

ede/dt	VS	S	M	L	VL
VS	VS	VS	VS	S	M
S	VS	VS	S	M	L
M	VS	S	M	L	VL
L	S	M	L	VL	VL
VL	M	L	VL	VL	VL

Property d: $\Phi(e_1,0) = \Rightarrow e_1 = 0$

Property e: $\Phi(.,.)$ corresponds to a sectorial function where for every scalar input there exists a solution $\lambda^{'}$, $\gamma^{'} > 0$ given by:

$$0 \le e_1[\Phi(e_1,e_2) - \Phi(0,e_2)] \le \lambda^{'} e_1^2 \tag{19}$$

$$0 \le e_2[\Phi(e_1,e_2) - \Phi(e_1,0)] \le \gamma^{'} e_2^2 \tag{20}$$

where λ and γ are constants.

The proof for the above properties is detailed in [46].

Hence, a continuous-time system with state vector $x \in R^n$, input $y(.) : R \to R$, and output $u(.) : R \to R$ is passive if there exists a real-valued storage function $V(x)$ which is continuous non-negative with $V(0) = 0$ and supply rate $W(y(\tau), u(\tau)) = y(\tau)u(\tau)$, to the extent that the subsequent dissipation inequality holds $\forall t > 0, u \in U, x(0) \in X$:

$$V(x(t)) - V(x(0)) \le \int_0^t W(y(\tau), u(\tau))d\tau \tag{21}$$

where, u is the control decision.

If the supply rate is:

$W(y(\tau), u(\tau)) = y(\tau), u(\tau) - \varepsilon y(\tau)^2$, $\varepsilon > 0$, input strictly passive system.

$W(y(\tau), u(\tau)) = y(\tau), u(\tau) - \varepsilon u(\tau)^2$, $\varepsilon > 0$, output strictly passive system.

$W(y(\tau), u(\tau)) = y(\tau), u(\tau) - \varepsilon_1 y(\tau)^2 - \varepsilon_2 u(\tau)^2$; $\varepsilon_1, \varepsilon_2 > 0$, input, and output strictly passive system.

Proof: Consider the generalized representation of the continuous-time system driven by a fuzzy controller with state access:

$$\dot{x} = f(x) + G(x)u \tag{22}$$

$$\zeta = h(x) \tag{23}$$

$$\dot{y} = \zeta \tag{24}$$

$$u = \Phi(e_1, e_2) \tag{25}$$

$$e(t) = y_d - y(t) \tag{26}$$

where, $x \in X \subset R^n$, $\zeta \in R$, $u \in R$, and $f(x) : X \to R^n$, $f(0) = 0$, $G(x) : X \to R^n$, $h(x) : X \to R$, $h(0) = 0$ are smooth functions, e_1 corresponds to the error between measured and desired outputs y and y_d, respectively, e_2 is the rate of change of error e_1, and $\Phi : R \times R \to R \in C^1$ corresponds to the control function. A basic assumption is made about the complete reachability and zero-state detectability of the system by following the above properties as follows:

$$u(t) = 0, \text{ and } \zeta(t) = 0 \Rightarrow \lim_{t \to \infty} x(t) = 0 \tag{27}$$

This assumption is obvious considering that the origin is an equilibrium point. Further, properties b and e lead to:

$$0 \le e_1 \Phi(e_1,0) \le \lambda^{'} e_1^2 \tag{28}$$

$$0 \le e_2 \Phi(0,e_2) \le \gamma^{'} e_2^2 \tag{29}$$

Let

$$\Delta_{e_2}(e_1, e_2) = \Phi(e_1,e_2) - \Phi(e_1,0) \tag{30}$$

$$\Delta_{e_1}(e_1, e_2) = \Phi(e_1,e_2) - \Phi(0, e_2) \tag{31}$$

This infers that

$$0 \le e_2 \Delta_{e_2}(e_1,e_2) \le \gamma^{'} e_2^2 \tag{32}$$

$$0 \le e_1 \Delta_{e_1}(e_1, e_2) \le \lambda^{'} e_1^2 \tag{33}$$

From the definition of passivity, the scalar control inputs result in

$$\begin{aligned} \int_0^t e_2(\tau)\Phi(e_1(\tau), e_2(\tau))d\tau &= \int_0^t e_1(\tau)\Phi(e_1(\tau), 0)d\tau \\ &\quad + \int_0^t e_2(\tau)\Delta_{e_2}(e_1(\tau), e_2(\tau))d\tau \\ &\ge V[e_1(t)] - V[e_1(0)] \end{aligned} \tag{34}$$

where

$$V[e_1(t)] - V[e_1(0)] = \int_0^t e_1(\tau)\Phi(e_1((\tau)),0)d\tau = \int_{e_1(0)}^{e_1(t)} \Phi(e_1,0)de_1 \tag{35}$$

This identifies that in a continuous domain the fuzzy controller is input-output passive stable.

The advantage of the passivity approach-based stability analysis is shown by plotting the state trajectory of the system with wavelet fuzzy controller in Fig. 5. As noted, the trajectory shows less oscillations with the action of wavelet transform while optimizing the fuzzy controller indicating a significant improvement in the performance of the system. Further, the figure reveals that all the rules of the wavelet fuzzy controller cover all the variations occurring in the system.

3.6. Digital realization of controller using FPGA technology

FPGA devices are aimed in the implementation of high performance, large size circuits, thanks to the speed advantage of direct hardware execution on the FPGA. With the increase in advancement of electronic design automation technology, FPGAs have started to receive more attention before due to its high compactness and high speed. In addition, the viability of modular design makes FPGA accomplish new and complex algorithms like neural networks, fuzzy logic algorithm, etc., [47]. Another important factor in using FPGAs is their re-configurability and reusable hardware architectures for rapid prototyping of the digital system.

The proposed wavelet-based fuzzy controller implemented in the Altera DE-II 115 FPGA board using Quartus II programming platform [48] to generate five different gating signals suitable to drive the switches of the system. The process of designing a wavelet fuzzy controller in an FPGA involves three major steps: fuzzification, rule evaluation, and defuzzification. In fuzzification, the WT provides inputs to the fuzzy system by classifying the voltage change in the system with

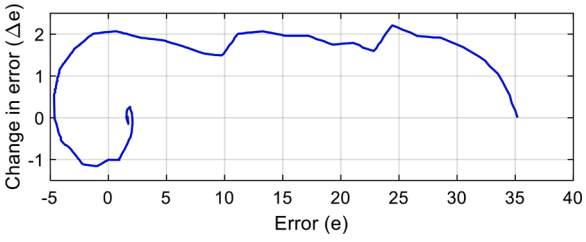

Fig. 5. State trajectory for passivity approach stability analysis of wavelet fuzzy controller.

respect to a prefixed reference voltage. The error and change in error points required for the input of fuzzy were obtained from the sampling and reconstruction process. In this design, the fuzzification contains two input membership functions, and each membership function outputs one corresponding grade when the input value is detected. Trapezoidal and triangular type formation is used for defining small (S [7…0]), medium (M [7…0]) and large (L [7…0]) representations of linguistic variables. The Rule evaluator is the second stage of the FLC. It contains a rule base with 25 rules. Here, AND and NOT operators are used for the antecedent of rules. Thus the "find max" function and "find min" function should be built at first place for the rule evaluator. The "not" function is a built-in function and can be called directly. The defuzzifier is the third stage of the FLC. It converts the fuzzy values into a crisp value for output through weighted averages as the defuzzification process. This method only involves additive and division, which makes the VHDL coding more applicable. After the individual design process, the last step is to connect them together. The VHDL code was successfully synthesized and the Modelsim simulation software was used to verify the digital realization of the proposed control strategy. The developed controller is programmed onto the board by communicating the computer and FPGA chip using a JTAG interface.

The DE2 FPGA board is utilized in this project. The process in loop for the development of the above control approach is shown in Fig. 6. The task is to load the VHDL program to the FPGA, after loading the program on the kit and carrying out the assignment of the output pulses to the GPIO of the board we have connected the GPIO ports of the FPGA board an oscilloscope to be able to experimentally examine the outputs. Before being able to download the VHDL program simulated in MODELSIM the Quartus software must be used in order to be able to download the last to the FPGA where the program must be compiled in the Quartus environment. Programmable logic device design software produced by Altera. Quartus enables analysis and synthesis of HDL designs, which enables the developer to compile their designs, perform timing analysis, simulate a design's reaction, and configure the target device with the programmer. Quartus includes an implementation of VHDL and Verilog for hardware description, visual editing of logic circuits, and vector waveform simulation. in here the sole purpose we needed Quartus software is to load our VHDL code to the FPGA board.

4. Results

To verify the analysis of the two-stage single-phase standalone PV system and its control as discussed in the above sections, simulation analysis has been carried out by using the schematic depicted in Fig. 1. The PV array is operated under standard test conditions (STC) of 1000 W/m^2 irradiance and 25 ^0C temperature for varying load conditions. The parameters of the simulated PV system can be found in Table 1. Since the simulation adapts STC and due to the action of the boost converter, the voltage across the DC link is maintained around 430 V to feed the input terminals of the inverter as depicted in Fig. 7. Further, the wavelet fuzzy controller is connected in closed loop with the inverter to demonstrate the controllability of the system.

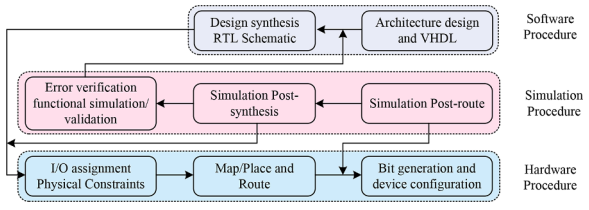

Fig. 6. Design flow of Field Programmable Gate Array (FPGA) for implementing the control approach.

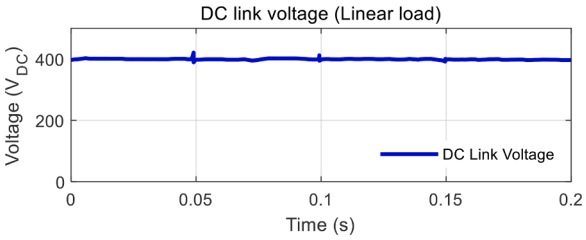

Fig. 7. DC link voltage at the input terminals of the inverter operating with varying linear load.

4.1. Simulation results

To validate the action of the developed controller in regulating the voltage, the simulations were carried out with 1 kWp variable linear and nonlinear loads. The results obtained with the nonlinear loads estimate the operating efficiency of the developed controller as they produce harmonics in load voltage by drawing harmonic currents through the output impedance. Generally, as specified by various standards a variation of up to 6% in the nominal voltage and a THD limit up to 5% is acceptable in load voltage and current [49].

Fig. 8 demonstrates the load voltage (Fig. 8a) and load current (Fig. 8b) for linear load operation. Initially, the system is operated with a 0.24 kWp load. The initial transients in the load current indicate that the system has initiated its operation in standalone mode, or it has shifted its operation from a grid connected mode to an islanded mode. Further, at $t = 0.5\ s$, the load is increased to 0.33 kWp, and a slight transient in load voltage is observed due to the load variation which is mitigated by the action of controller. At $t = 1\ s$ and $t = 1.5\ s$, the load is increased to 0.45 kWp and 0.84 kWp, respectively. The results showed the effectiveness of developed controller in regulating the transients in the voltage during load variation. The total harmonic distribution and the fundamental component of voltage and current are shown in Fig. 9(a) and (b). The harmonics are displayed as the magnitude of the fundamental component in percentage. The highest harmonic for load voltage appears to be > 2 % at 50 Hz resulting in 2.18 % THD and the highest harmonic for load current appears to be > 0.06 % at 50 Hz resulting in 3.47 % THD.

Fig. 10 demonstrates the load voltage (Fig. 10a) and load current (Fig. 10b) for nonlinear load. The nonlinear load is realised by connecting a rectifier along with a 1 kWp resistive load. Initially, the system is operated with a 0.5 kWp load. The initial transients in the load voltage and load current indicate that the system has initiated its operation in standalone mode, or it has shifted its operation from a grid connected mode to an islanded mode. Further, at $t = 0.5\ s$, the load is increased to 0.58 kWp, and a slight transient in load voltage is observed due to the load variation which is mitigated by the action of controller. At $t = 1\ s$ and $t = 1.5\ s$, the load is increased to 0.7 kWp and 0.87 kWp respectively.

The results showed the effectiveness of developed controller in regulating the transients in the voltage during load variation. The total harmonic distribution and the fundamental component of voltage and current are shown in Fig. 11(a) and (b). The highest harmonic for load voltage appears to be 4 % at 50 Hz resulting in 3.74 % THD and the highest harmonic for load current appears to be > 0.06 % at 50 Hz resulting in 4.86 % THD. Further, the superiority of the controller is assessed by calculating the overshoot, and steady state error for different controllers under varying load conditions as shown in Table 3.

4.2. Test results

To assess the action of the developed controller on a single-phase standalone PV system, experimental tests are carried out by using the laboratory setup. The PV arrays with the rated power of 1 kW are

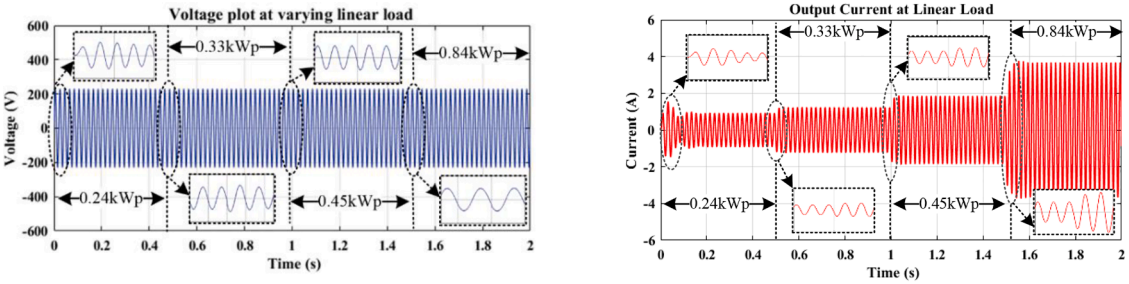

(a) Voltage output for linear load variation. (b) Current output for linear load variation.

Fig. 8. Load voltage and load current for operation of PV system with linear load.

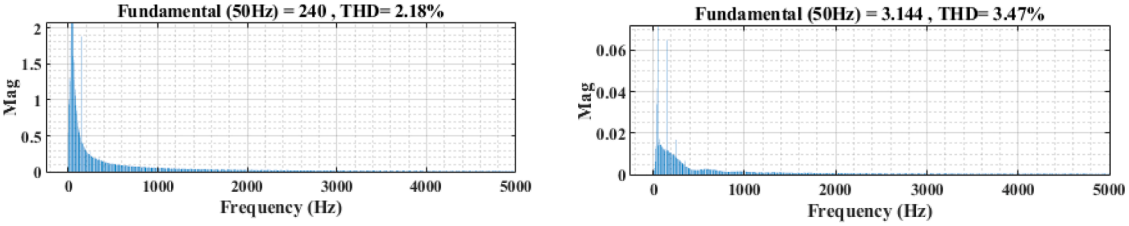

(a) FFT analysis for load voltage (b) FFT analysis for load current

Fig. 9. FFT analysis for PV system operating at 100% linear load.

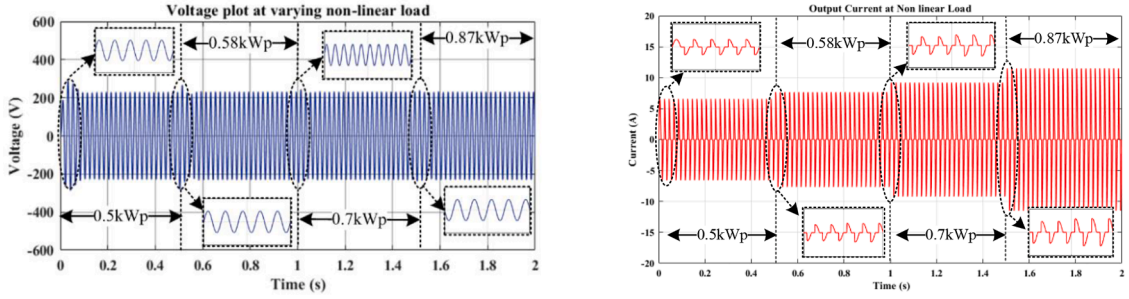

(a) Voltage output for non-linear load variation. (b) Current output for non-linear load variation.

Fig. 10. Load voltage and load current for operation of PV system with linear load.

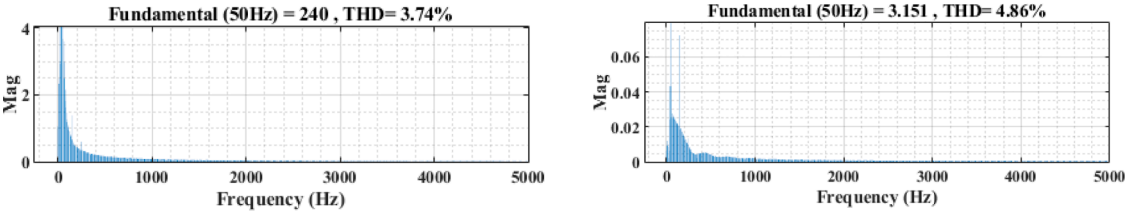

(a) FFT analysis for load voltage (b) FFT analysis for load current

Fig. 11. FFT analysis for PV system operating at 100% non-linear load.

Table 3
Comparison between performance parameters of different controllers for voltage regulation.

Controller	Overshoot (%)		Steady State Error	
Load	No	Full	No	Full
FLC (Linear Load)	1.2	1.8	0.4	0.8
Wavelet FLC (Linear Load)	0	0	0.2	0.3
FLC (Non-Linear Load)	2.02	3.35	1.2	1.8
Wavelet FLC (Non-Linear Load)	0	0.6	0.7	0.9

realized by using a PV simulator, which can emulate the behavior of the PV arrays according to the PV cell parameters and the irradiance profile. The parameters of the single-phase standalone PV system can be found in Table 1. The digital controller is developed in the FPGA platform, as discussed in Section 3.5. The main goal of this section is to illustrate the controllability of the single-phase standalone PV system through the setup shown in Fig. 12.

The experimental analysis is performed on the laboratory prototype along with the digital controller for a linear resistive load and a rectifier load which acts as a nonlinear load. Initially, the system is operated with 1 *kWp* linear load and the corresponding characteristics are observed as shown in Figs. 13 and 14.

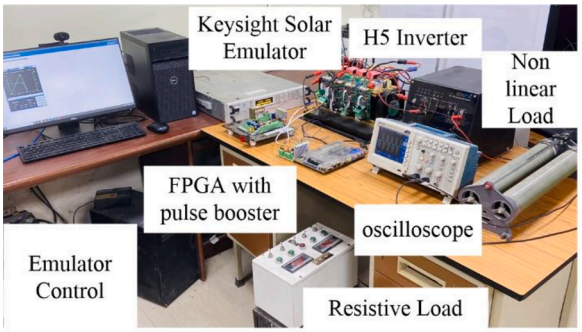

Fig. 12. Experimental setup for standalone operation of PV inverter with developed controller.

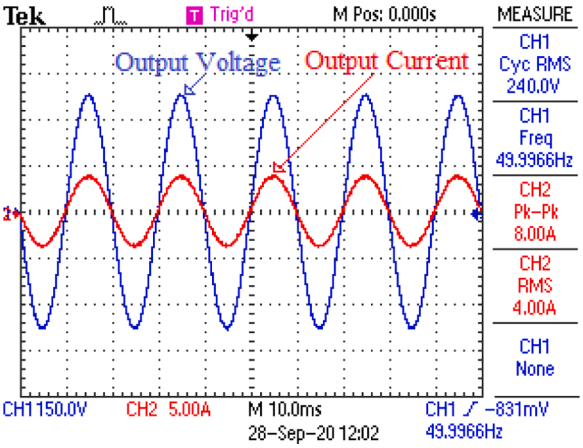

Fig. 13. Load voltage and load current for standalone operation of PV system with 1kWp load.

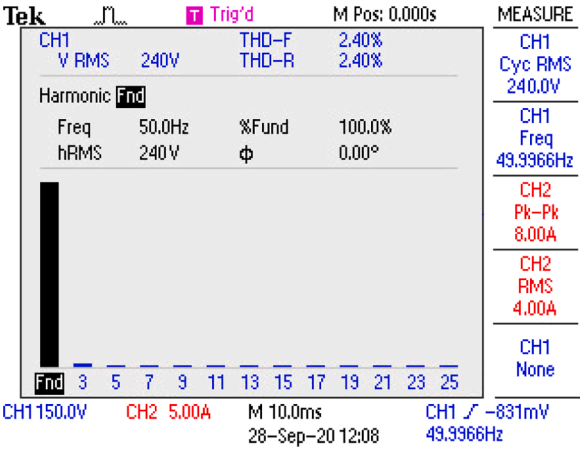

Fig. 14. THD of load voltage for standalone operation of PV system with 1kWp load.

In Fig. 13 the peak voltage of the system and load current operating under normal conditions is observed. The results showed the smooth action of controller while operating with full load. The THD of load voltage for standalone operation of PV system with 1 *kWp* load.is observed to be around 2.4 %. Further, the inverter is subjected to operate in no load condition and at time *t*, the load relates to the system under no load operation. At this instant, the developed controller acts instantaneously by regulating the load voltage to operate in the specified limit and the corresponding characteristics are observed as shown in

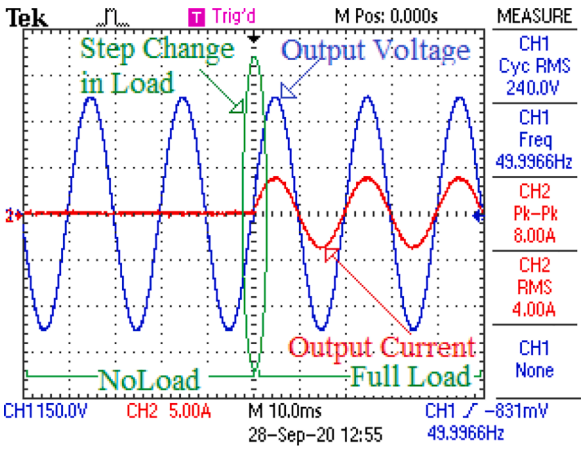

Fig. 15. Load voltage and load current for standalone operation of PV system under varying load.

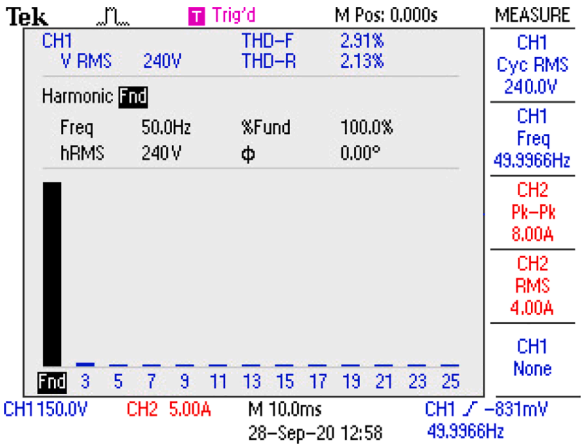

Fig. 16. THD of Load voltage for standalone operation of PV system under varying load.

Figs. 15 and 16. The results showed the peak voltage and load current during the action of developed controller while operating with load variation. The initial action of the controller is observed with no load operation and at $t = 50\ ms$, a 1 *kWp* load is switched with the inverter. The developed controller efficiently supresses the transients in voltage maintaining smooth and steady state operation. The THD of load voltage for standalone operation of PV system under varying load is observed to be around 2.9 %.

Further, the inverter is operated with a rectifier controlled resistive load to depict the operation of the digitally realised controller on the nonlinear load. The peak voltage and load current during the operation of PV system for a 1 *kWp* load is shown in Fig. 17. In addition, the FFT analysis for the voltage of the inverter operating with nonlinear load is observed to be 4.71 %, as shown in Fig. 18. Table 4 indicates the voltage THD for different loads under simulated and experimental conditions.

Fig. 19 depicts the comparisons between efficiencies of the controlled inverter topology and the conventional inverter topologies depicted in [7,8]. It is observed that the efficiency of the proposed inverter is higher than that of the literature. A comparitive analysis of various parameters of the developed controller on H5 inverter are presented with various topologies in the literature is shown in Table 5. The results depicted efficient operation of the inverter with reduced THD.

The results showed the improved performance of the inverter with the developed controller. The transients in voltage for load switching were regulated efficiently by the developed controller, resulting in reduced THD. Further, the developed approach has the following

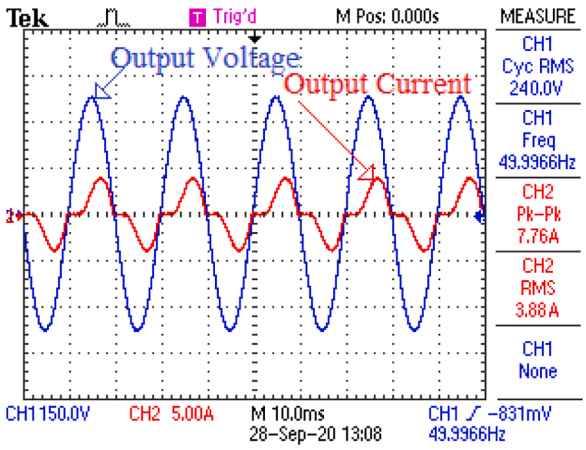

Fig. 17. Steady state response of inverter under standalone operation with 1kWp nonlinear load.

Fig. 18. THD of inverter voltage output operating under 1kWp nonlinear load.

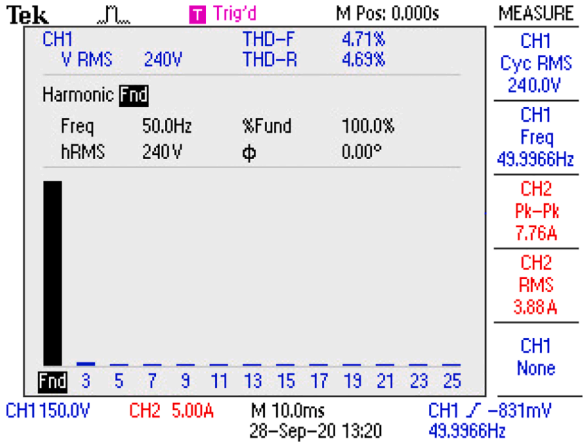

Fig. 18. THD of inverter voltage output operating under 1kWp nonlinear load.

Table 4
Voltage THD for simulated and experimented systems.

Load	Simulation	Experiment
Linear	2.18%	2.4%
Non-Linear load	3.74%	4.71%

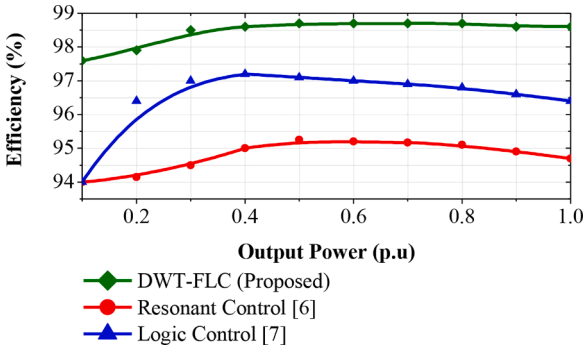

Fig. 19. Calculated efficiency for controlled inverter topology.

Table 5
Comparison between simulation and experimental results.

Parameter	H5 Transformerless Inverter	Switched capacitor based Inverter [5]	MLI Inverter [10]
RMS Voltage	240*V*	230*V*	110*V*
Topology	1Phase, H5	Switched Capacitor base inverter	1 Phase, Multi-Level
Control Technique Implemented	Wavelet Fuzzy	proportional–integral-based closed-loop control	Vector Control
Voltage THD	2.4% (Linear Full load)	<4%	2.4%
Efficiency	98.5%	>85%	9.75%

drawbacks:

- Thresholding is not applied for the scaling functions.
- Specific disturbances in the signal may not match with the chosen mother wavelet resulting in irregular firing of fuzzy rules.

These drawbacks can be overcome by adapting various thresholding techniques and developing flexible mother wavelet functions.

5. Conclusion

The work presented in this paper develops a wavelet fuzzy based controller for standalone operation of single-phase PV inverter system. The proposed system is simulated in MATLAB/Simulink environment and evaluated for Voltage regulation and THD with varying linear and nonlinear loads. The results depicted balanced voltage regulation for varying load conditions and achieved THD of 2.18 % while operating with linear loads, 3.74 % for nonlinear loads. Further, the developed control strategy is assessed with a 1 *kW* laboratory prototype. The developed model is evaluated for voltage regulation under full load, no load and step change in load conditions. The developed control achieves output voltage regulation both in steady state and transient conditions with a minimum voltage THD of 2.4 % for linear load and 4.7 % for nonlinear load. Further, the research can be extended by developing the DWT-based voltage loop control for grid connected operation in a single-phase network, and for voltage regulation and grid connected operation of a three-phase converter.

Declaration of Competing Interest

The authors declare that they have no known competing financial interests or personal relationships that could have appeared to influence the work reported in this paper.

Data availability

No data was used for the research described in the article.

References

[1] J. Selvaraj, N.A. Rahim, Multilevel Inverter For Grid-Connected PV System Employing Digital PI Controller, IEEE Trans. Ind. Electron. 56 (1) (2009) 149–158, https://doi.org/10.1109/TIE.2008.928116. Jan.
[2] M.E. Haque, M. Negnevitsky, K.M. Muttaqi, A Novel Control Strategy for a Variable-Speed Wind Turbine With a Permanent-Magnet Synchronous Generator, IEEE Trans. Ind. Appl. 46 (1) (2010) 331–339, https://doi.org/10.1109/TIA.2009.2036550.
[3] M.A. Khan, A. Haque, V.S.B. Kurukuru, M. Saad, Islanding detection techniques for grid-connected photovoltaic systems-A review, Renew. Sustain. Energy Rev. 154 (Feb. 2022), 111854, https://doi.org/10.1016/j.rser.2021.111854.
[4] M. Yazdanian, A. Mehrizi-Sani, Case Studies on Cascade Voltage Control of Islanded Microgrids Based on the Internal Model Control, IFAC-PapersOnLine 48 (30) (2015) 578–582, https://doi.org/10.1016/j.ifacol.2015.12.442.

[5] D. Debnath, K. Chatterjee, Solar photovoltaic-based stand-alone scheme incorporating a new boost inverter, IET Power Electron 9 (4) (2016) 621–630, https://doi.org/10.1049/iet-pel.2015.0112. Mar.
[6] O.V. Kulkarni, S. Doolla, B.G. Fernandes, Mode Transition Control Strategy for Multiple Inverter-Based Distributed Generators Operating in Grid-Connected and Standalone Mode, IEEE Trans. Ind. Appl. 53 (6) (2017) 5927–5939, https://doi.org/10.1109/TIA.2017.2743682. Nov.
[7] Y.-.C. Liu, M.-.C. Chen, C.-.Y. Yang, K. Kim, H.-.J. Chiu, High-Efficiency Isolated Photovoltaic Microinverter Using Wide-Band Gap Switches for Standalone and Grid-Tied Applications, Energies 11 (3) (2018) 569, https://doi.org/10.3390/en11030569. Mar.
[8] R.Y. Duan, C.T. Chang, A novel high-efficiency inverter for stand-alone and grid-connected systems, in: 2008 3rd IEEE Conf. Ind. Electron. Appl. ICIEA 2008, 2008, pp. 557–562, https://doi.org/10.1109/ICIEA.2008.4582577.
[9] D. Leng, S. Polmai, Transient Respond Comparison Between Modified Droop Control and Virtual Synchronous Generator in Standalone Microgrid, in: 2019 5th International Conference on Engineering, Applied Sciences and Technology (ICEAST), 2019, pp. 1–4, https://doi.org/10.1109/ICEAST.2019.8802552. Jul.
[10] N. Kumar, T.K. Saha, J. Dey, Multilevel Inverter (MLI)-Based Stand-Alone Photovoltaic System: modeling, Analysis, and Control, IEEE Syst. J. (2019) 1–7, https://doi.org/10.1109/jsyst.2019.2900485. Mli.
[11] R.O. Ramirez, et al., Predictive controller for a three-phase/single-phase voltage source converter cell, IEEE Trans. Ind. Informatics 10 (3) (2014) 1878–1889, https://doi.org/10.1109/TII.2014.2332062.
[12] Y. Cho, J.-S. (Jason) Lai, "Digital Plug-In Repetitive Controller for Single-Phase Bridgeless PFC Converters, IEEE Trans. Power Electron. 28 (1) (2013) 165–175.
[13] Dong-Eok Kim, Dong-Choon Lee, Feedback Linearization Control of Three-Phase UPS Inverter Systems, IEEE Trans. Ind. Electron. 57 (3) (2010) 963–968, https://doi.org/10.1109/tie.2009.2038404.
[14] A. Houari, H. Renaudineau, J.-.P. Martin, S. Pierfederici, F. Meibody-Tabar, Flatness-Based Control of Three-Phase Inverter With Output LC Filter, IEEE Trans. Ind. Electron. 59 (7) (2012) 2890–2897, https://doi.org/10.1109/TIE.2011.2170396. Jul.
[15] M. Aamir, K.A. Kalwar, S. Mekhilef, Proportional-Resonant and Slide Mode Control for Single-Phase UPS Inverter, Electr. Power Components Syst. 45 (1) (2017) 11–21, https://doi.org/10.1080/15325008.2016.1233301.
[16] Y. Elthokaby, I. Abdelsalam, N. Abdel-Rahim, I. Mohamed, Standalone PV-based single-phase split-source inverter using model-predictive control, Alexandria Eng. J. 62 (2023) 357–367, https://doi.org/10.1016/j.aej.2022.07.035. Jan.
[17] I. Al-Wesabi, Z. Fang, Z. Wei, H. Dong, Direct Sliding Mode Control for Dynamic Instabilities in DC-Link Voltage of Standalone Photovoltaic Systems with a Small Capacitor, Electronics (Basel) 11 (1) (2022) 133, https://doi.org/10.3390/electronics11010133. Jan.
[18] A. Yadav, V.K. Deolia, S. Agrawal, Indirect closed loop control of quasi-Z-source inverter for standalone solar PV-based energy conversion system, Int. J. Power Energy Convers. 12 (3) (2021) 236, https://doi.org/10.1504/IJPEC.2021.116579.
[19] P. Nithara, R.P. Eldho, Comparative Analysis of Different Control strategies in Single phase Standalone Inverter, in: 2021 7th International Conference on Advanced Computing and Communication Systems (ICACCS), 2021, pp. 1105–1109, https://doi.org/10.1109/ICACCS51430.2021.9441547. Mar.
[20] D.K. Setiawan, M. Ashari, H. Suryoatmojo, Harmonics Reduction for Four-Leg Distribution Network-Connected Single Phase Transformerless PV Inverter System Using Diagonal Recurrent Neural Network, in: 2019 International Conference of Artificial Intelligence and Information Technology (ICAIIT), 2019, pp. 331–335, https://doi.org/10.1109/ICAIIT.2019.8834462. Mar.
[21] M.A. Khan, A. Haque, V.S.B. Kurukuru, Intelligent control of a novel transformerless inverter topology for photovoltaic applications, Electr. Eng. 102 (2) (2020) 627–641, https://doi.org/10.1007/s00202-019-00899-2. Jun.
[22] M.A. Hannan, J.A. Ali, A. Mohamed, M.N. Uddin, A Random Forest Regression Based Space Vector PWM Inverter Controller for the Induction Motor Drive, IEEE Trans. Ind. Electron. 64 (4) (2017) 2689–2699, https://doi.org/10.1109/TIE.2016.2631121. Apr.
[23] S. Vedantham, S. Kumar, B. Singh, S. Mishra, Fuzzy logic gain-tuned adaptive second-order GI-based multi-objective control for reliable operation of grid-interfaced photovoltaic system, IET Gener. Transm. Distrib. 12 (5) (2018) 1153–1163, https://doi.org/10.1049/iet-gtd.2017.0958. Mar.
[24] M.A. Khan, A. Haque, V.S.B. Kurukuru, H. Wang, F. Blaabjerg, Stand-Alone Operation of Distributed Generation Systems With Improved Harmonic Elimination Scheme, IEEE J. Emerg. Sel. Top. Power Electron. 9 (6) (2021) 6924–6934, https://doi.org/10.1109/JESTPE.2021.3084737. Dec.
[25] M.A. Khan, A. Haque, V.S.B. Kurukuru, Performance assessment of stand-alone transformerless inverters, Int. Trans. Electr. Energy Syst. 30 (1) (2020), https://doi.org/10.1002/2050-7038.12156. Jan.
[26] S.A. Saleh, M.A. Rahman, Analysis and Real-Time Testing of a Controlled Single-Phase Wavelet-Modulated Inverter for Capacitor-Run Induction Motors, IEEE Trans. Energy Convers. 24 (1) (2009) 21–29, https://doi.org/10.1109/TEC.2008.2003214. Mar.
[27] S.A. Saleh, M.A. Rahman, Development and Testing of a New Controlled Wavelet-Modulated Inverter for IPM Motor Drives, IEEE Trans. Ind. Appl. 46 (4) (2010) 1630–1643, https://doi.org/10.1109/TIA.2010.2049814. Jul.
[28] S.A. Saleh, M.A. Rahman, Development and Experimental Validation of Resolution-Level Controlled Wavelet-Modulated Inverters for Three-Phase Induction Motor Drives, IEEE Trans. Ind. Appl. 47 (4) (2011) 1958–1970, https://doi.org/10.1109/TIA.2011.2156375. Jul.
[29] Jinlong Zhang, Yanjun Wei, Xiangli Li, Hanhong Qi, Inverter control technology based on multi-resolution wavelet modulation, in: 2014 IEEE Conference and Expo Transportation Electrification Asia-Pacific (ITEC Asia-Pacific), 2014, pp. 1–5, https://doi.org/10.1109/ITEC-AP.2014.6940890. Aug.
[30] T. Esram, P.L. Chapman, Comparison of Photovoltaic Array Maximum Power Point Tracking Techniques, IEEE Trans. Energy Convers. 22 (2) (2007) 439–449, https://doi.org/10.1109/TEC.2006.874230. Jun.
[31] P. Sindhuja, V.U. Reddy, Enhancement of grid connected PV inverter using optimal maximum power point tracking algorithm with estimation of climatic parameter, in: 2017 International Conference on Inventive Systems and Control (ICISC), 2017, pp. 1–6, https://doi.org/10.1109/ICISC.2017.8068623. Jan.
[32] M. et al. Victor, "US Patent Application-H5 Inverter (SMA)," 0286281 A1, 2005.
[33] T. Kerekes, "Analysis and Modeling of Transformerless Photovoltaic Inverter," 2013.
[34] A.J. Babqi, Z. Yi, D. Shi, X. Zhao, Model Predictive Control of H5 Inverter for Transformerless PV Systems with Maximum Power Point Tracking and Leakage Current Reduction, in: *IECON 2018 - 44th Annu. Conf. IEEE Ind. Electron. Soc.*, no. Iecon, 2018, pp. 1860–1865, https://doi.org/10.1109/IECON.2018.8591386. Oct.
[35] M. Jayaraman, V.T. Sreedevi, Implementation of LC and LCL passive filters for harmonic reduction in PV based renewable energy systems, in: 2017 National Power Electronics Conference (NPEC), 2017, pp. 363–369, https://doi.org/10.1109/NPEC.2017.8310486. Dec.
[36] M. Liserre, F. Blaabjerg, S. Hansen, Design and Control of an LCL-Filter-Based Three-Phase Active Rectifier, IEEE Trans. Ind. Appl. 41 (5) (2005) 1281–1291, https://doi.org/10.1109/TIA.2005.853373. Sep.
[37] A. Reznik, M.G. Simoes, A. Al-Durra, S.M. Muyeen, LCL Filter Design and Performance Analysis for Grid-Interconnected Systems, IEEE Trans. Ind. Appl. 50 (2) (2014) 1225–1232, https://doi.org/10.1109/TIA.2013.2274612. Mar.
[38] J. Daya, V. Subbiah, A novel wavelet-fuzzy-based controller for robust speed control induction motor drives, Aust. J. Electr. Electron. Eng. 9 (2) (2012) 185–196, https://doi.org/10.7158/E11-919.2012.9.2.
[39] I.M. Dremin, O.V. Ivanov, V.A. Nechitailo, Wavelets and their uses, Physics-Uspekhi 44 (5) (2001) 447–478, https://doi.org/10.1070/PU2001v044n05ABEH000918. May.
[40] H. Morsheddost, D. Asemani, N. Mirahadi, Optimization of MDL-based wavelet denoising for fMRI data analysis, in: 2014 IEEE 11th International Symposium on Biomedical Imaging (ISBI), 2014, pp. 33–36, https://doi.org/10.1109/ISBI.2014.6867802. Apr.
[41] S. (ILLC) de Rooij, *Minimum Description Length Model Selection Problems and Extensions*. 2008.
[42] S. Parvez, Z. Gao, A wavelet-based multiresolution PID controller, IEEE Trans. Ind. Appl. 41 (2) (2005) 537–543, https://doi.org/10.1109/TIA.2005.844378.
[43] J.L. Febin Daya, V. Subbiah, A. Iqbal, S. Padmanaban, Novel wavelet-fuzzy based indirect field oriented control of induction motor drives, J. Power Electron. 13 (4) (2013) 656–668, https://doi.org/10.6113/JPE.2013.13.4.656.
[44] J.L. Febin Daya, V. Subbiah, P. Sanjeevikumar, Robust Speed Control of an Induction Motor Drive using Wavelet-fuzzy based Self-tuning Multiresolution Controller, Int. J. Comput. Intell. Syst. 6 (4) (2013) 724–738, https://doi.org/10.1080/18756891.2013.803741.
[45] G. Calcev, "A Passivity Result for Fuzzy Control Systems," vol. 61, no. December, pp. 2727–2728, 1996, doi: 10.1109/CDC.1996.573518.
[46] Y.C. Shin and Chengying Xu, "Stability Analysis Method," in *Automation and Control Engineering*, 1st ed., United States, 2008, pp. 225–235.
[47] Y. Bai et al., "FPGA vs DSP : a Throughput and Power Efficiency Comparison for Hierarchical Enumerative Coding," 2013.
[48] Y. Hong, S. Member, and I.J.G.F. Hsu, "Design and Realization of Controller for Static Switch in Microgrid Using Wavelet-based TSK Reasoning," vol. 3203, no. c, 2018, doi: 10.1109/TII.2018.2804896.
[49] National electrical code. 2011.

Mohammed Ali Khan (S'17-M'22) received his B.Tech. degree in Electrical and Electronics Engineering from Karunya University, Coimbatore, India, in 2013, and M.Tech. degree in Power System from Amity University, Noida, India, in 2016. He completed his Ph.D. degree in Power Management of Grid Connected Distribution Generation with the Advanced Power Electronics Research Laboratory, Department of Electrical Engineering, Jamia Millia Islamia (A Central University), New Delhi, India, in 2021. He is currently working as a Post-Doctoral Reseacher with the Department of Electrical Power Engineering, Faculty of Electrical Engineering and Communication, Brno University of Technology, Brno, Czech Republic. He was a Visiting Researcher at the Center of Reliable Power Electronics, Aalborg University, Aalborg, Denmark, from October to December 2020. He had also worked as Guest Faculty in the Department of Electrical Engineering, Jamia Millia Islamia (A Central University), New Delhi, India from 2017 to 2020. He has many publications in peer-reviewed journals and presented his research articles in several international conferences. His-area of research is artificial intelligence, power electronics, and their application in renewable energy systems, power quality improvements, and reliability.

Ahteshamul Haque (M'13-SM'14) received the B.Tech. degree in Electrical Engineering from Aligarh Muslim University, Aligarh, India, in 1999, the master's degree in Electrical Engineering from IIT Delhi, New Delhi, India, in 2000, and the Ph. D. degree in Electrical Engineering from the Department of Electrical Engineering, Jamia Millia Islamia University, New Delhi, India, in 2015. Prior to academics, he was working in the research and development unit of world reputed multinational industries and his work is patented in the USA and Europe. He is currently an Associate Professor with the Department of Electrical Engineering, Jamia Millia Islamia University. He has established Advance Power Electronics Research Laboratory, Department of Electrical Engineering, Jamia Millia Islamia. He is working as a Principal Investigator of the MHRD-SPARC project and other research and development projects. He is the recipient of IEEE PES Outstanding Engineer Award for the year 2019. He has authored or co-authored around 100 publications in international journals and conference proceedings. He is Senior Member of IEEE. His-current research interests include power converter topologies, control of power converters, renewable energy, and energy efficiency, reliability analysis, electric vehicle operations.

V S Bharath Kurukuru (S'18- M'22) received his B.Tech. degree in Electrical and Electronics Engineering from Avanthi's Research and Technological Academy, Vizianagaram, India, in 2014, and M.Tech. degree in Power Systems from Amity University, Noida, India, in 2016. He completed his Ph.D. degree in Intelligent Monitoring of Solar Photovoltaic System with the Advanced Power Electronics Research Laboratory, Department of Electrical Engineering, Jamia Millia Islamia (A Central University), New Delhi, India, in 2021. He is currently working as a Scientist (Packaging & Multiphysics) at Power Electronics Research Division, Silicon Austria Labs GmbH, Villach, Austria. He was a Visiting Researcher at the Center of Reliable Power Electronics, Aalborg University, Aalborg, Denmark, from August to October 2019. His-area of research is fault diagnosis, condition monitoring, and reliability of power electronics converters in renewable energy systems and electric vehicles.

Frede Blaabjerg (S'86–M'88–SM'97–F'03) was with ABB-Scandia, Randers, Denmark, from 1987 to 1988. From 1988 to 1992, he got the PhD degree in Electrical Engineering at Aalborg University in 1995. He became an Assistant Professor in 1992, an Associate Professor in 1996, and a Full Professor of power electronics and drives in 1998. From 2017 he became a Villum Investigator. He is honoris causa at University Politehnica Timisoara (UPT), Romania and Tallinn Technical University (TTU) in Estonia. His-current research interests include power electronics and its applications such as in wind turbines, PV systems, reliability, harmonics and adjustable speed drives. He has published more than 600 journal papers in the fields of power electronics and its applications. He is the co-author of four monographs and editor of ten books in power electronics and its applications.He has received 33 IEEE Prize Paper Awards, the IEEE PELS Distinguished Service Award in 2009, the EPE-PEMC Council Award in 2010, the IEEE William E. Newell Power Electronics Award 2014, the Villum Kann Rasmussen Research Award 2014, the Global Energy Prize in 2019 and the 2020 IEEE Edison Medal. He was the Editor-in-Chief of the IEEE TRANSACTIONS ON POWER ELECTRONICS from 2006 to 2012. He has been Distinguished Lecturer for the IEEE Power Electronics Society from 2005 to 2007 and for the IEEE Industry Applications Society from 2010 to 2011 as well as 2017 to 2018. In 2019–2020 he served as a President of IEEE Power Electronics Society. He has been Vice-President of the Danish Academy of Technical Sciences. He is nominated in 2014–2020 by Thomson Reuters to be between the most 250 cited researchers in Engineering in the world.